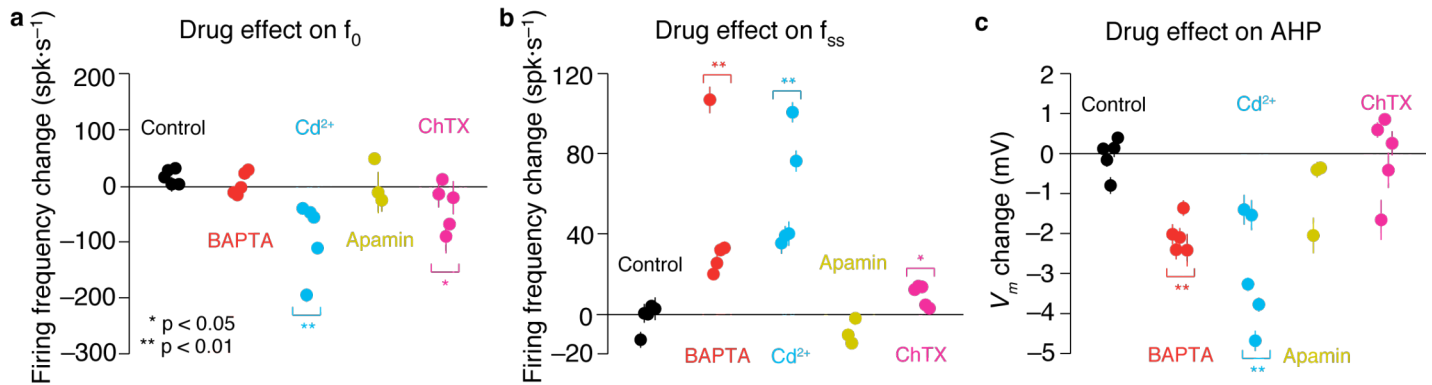
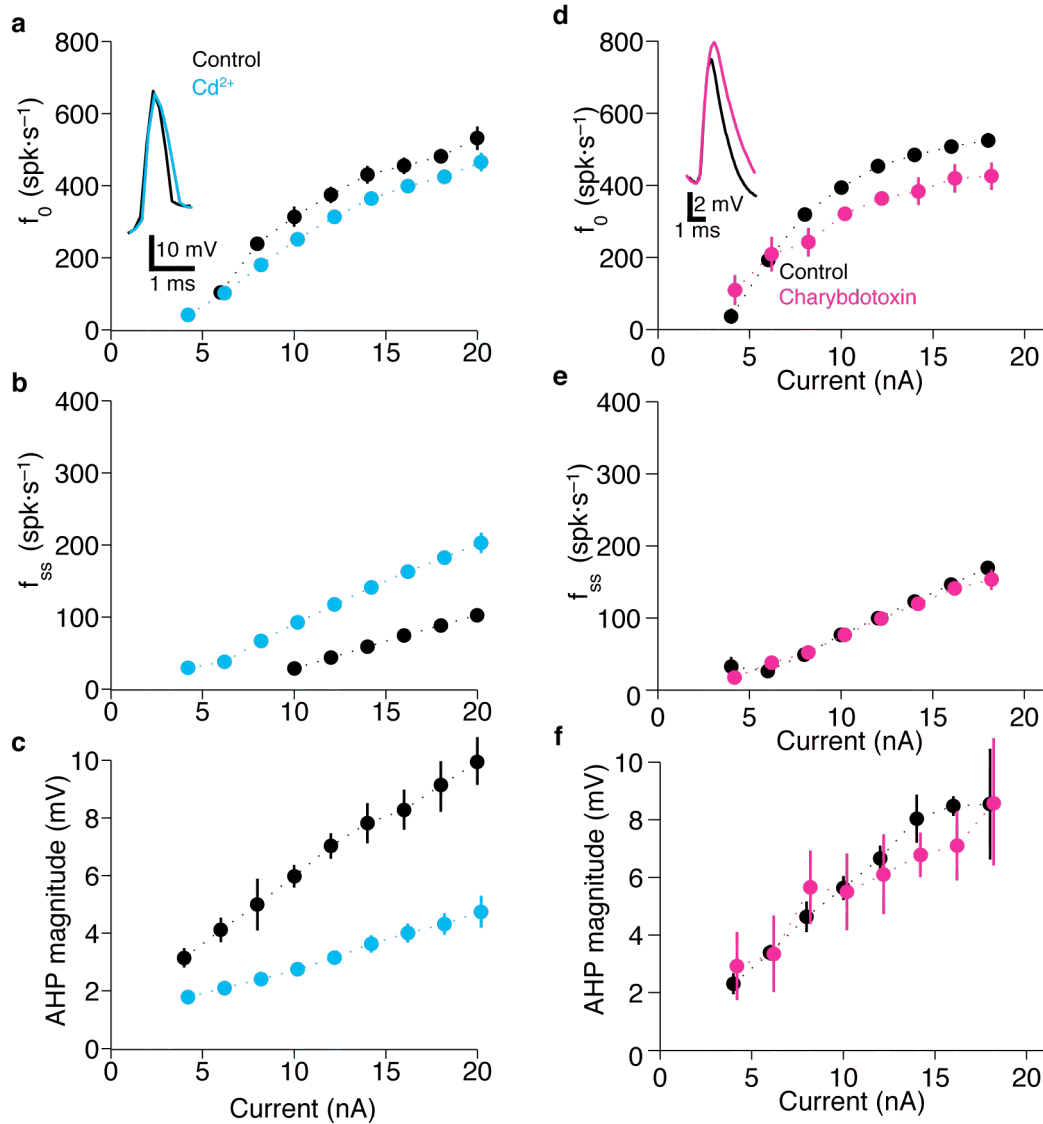


Spike Frequency Adaptation Mediates Looming Stimulus Selectivity in a Collision-Detecting Neuron

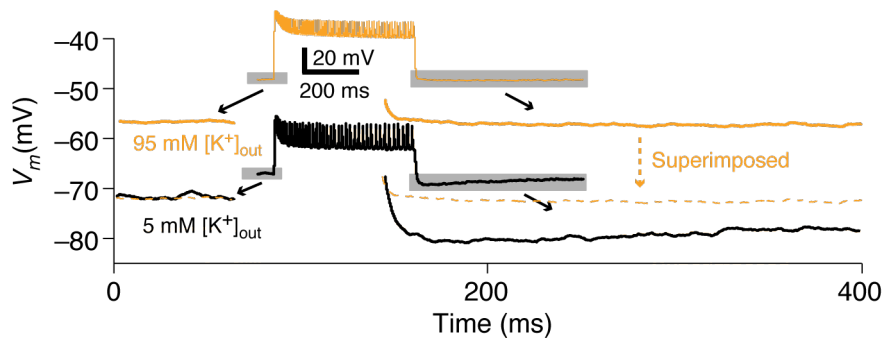
Simon Peron and Fabrizio Gabbiani



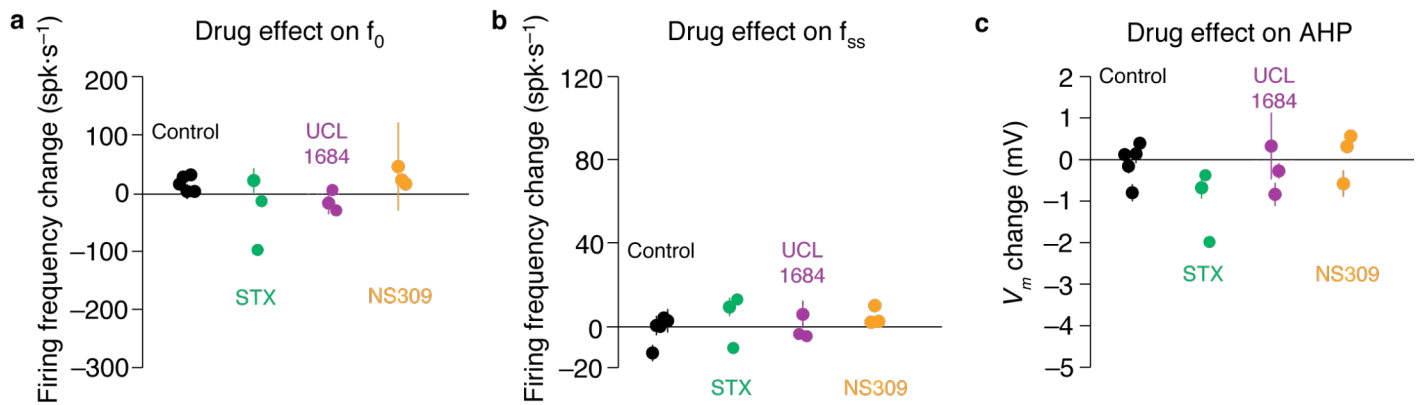
Supplementary Figure 1. Single cell summary of drug effects on values of SFA parameters. Each data point summarizes data from a single neuron and was obtained by averaging the absolute change of a particular parameter at every current level that elicited spiking. At least $N=5$ trials at each current level (and usually $N > 25$ trials with at least 5 current levels) were used for each animal (lines indicate s.e.m.). Change was considered significant if the average absolute change pooled across cells for a particular treatment differed from that observed with the rundown control (Wilcoxon rank-sum test). **(a)** Cd^{2+} and ChTX significantly reduced f_0 relative to control ($p = 0.008$ and $p = 0.032$, respectively; $N=5$ animals each). BAPTA and apamin did not yield significant changes ($p = 0.310$ and $p = 0.571$, respectively; $N=5$ and 3 animals, respectively). **(b)** BAPTA and Cd^{2+} gave rise to large increases in f_{ss} relative to control ($p = 0.008$ for both). ChTX yielded a much smaller increase ($p = 0.032$). Apamin did not produce a significant effect ($p = 0.143$). **(c)** BAPTA and Cd^{2+} gave rise to a large significant decrease in AHP magnitude ($p = 0.008$ for both), while apamin did not yield a significant change ($p = 0.143$).



Supplementary Figure 2. Effect of cadmium (Cd^{2+}) and charybdotoxin (ChTX) on spike frequency adaptation (SFA). In all cases, dots indicate the mean for a given current injection while lines indicate s.d.. A sample data set for a single animal with 10 repetitions per current injection level is shown for each treatment. **(a-c)** Cd^{2+} saline (Methods) has a similar effect on SFA as intracellular BAPTA, with the exception that f_0 declined slightly **(a)**, presumably due to action potential broadening (inset). This is consistent with block of a BK conductance. As with BAPTA iontophoresis (**Fig. 2d-e**), f_{ss} increased **(b)** and AHP magnitude declined **(c)**. **(d-f)** ChTX has effects consistent with a BK conductance block. f_0 declined **(d)** presumably due to widening of spikes (inset). As expected, neither f_{ss} **(e)** nor AHP **(f)** magnitude were affected by ChTX.

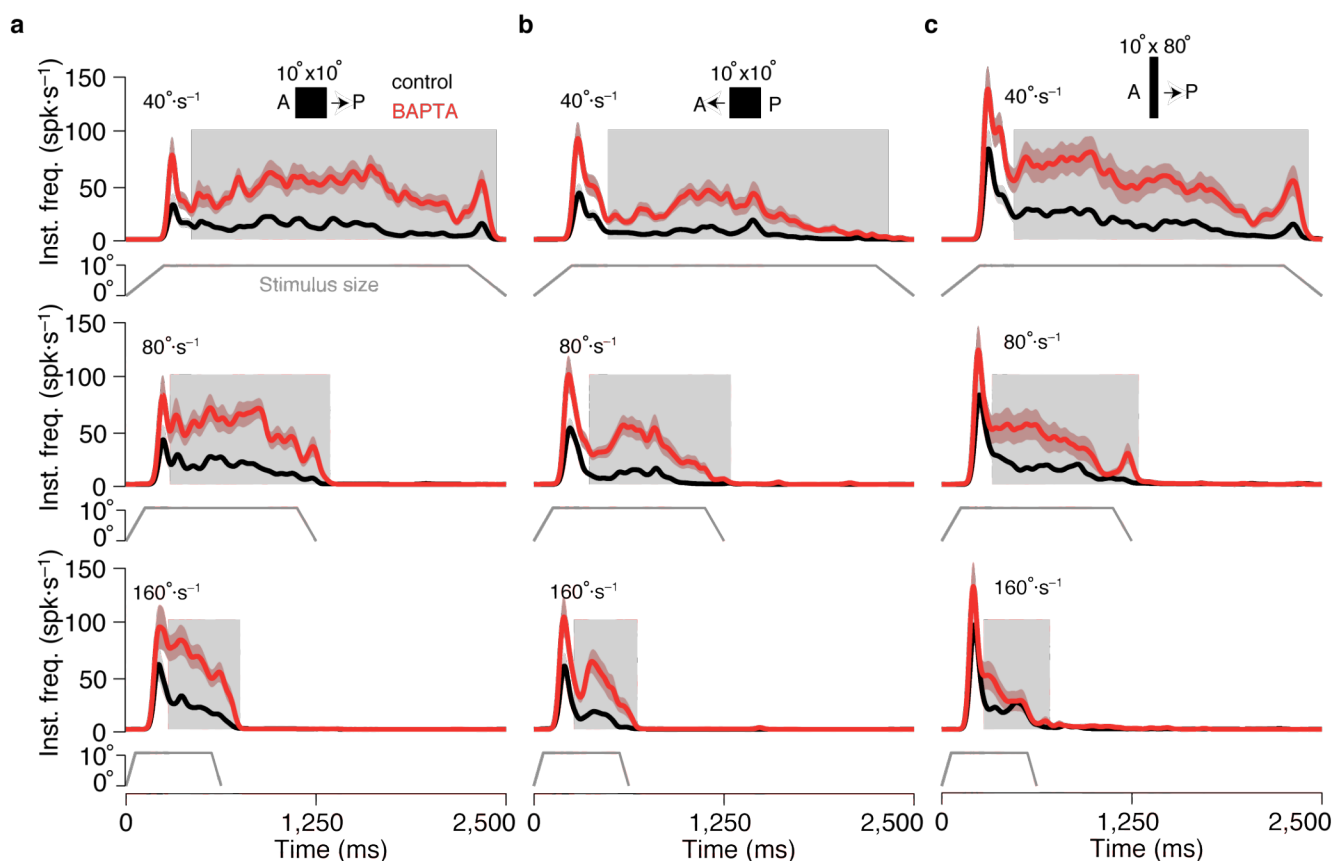


Supplementary Figure 3. In the LGMD, the after-hyperpolarization (AHP) related to spike frequency adaptation after depolarizing current pulses is K^+ dependent. Responses to a depolarizing current pulse (+13 nA) with a baseline hyperpolarizing current of -6 nA. In regular saline ($[K^+]_{out} = 5$ mM; black), a prominent AHP can be observed. Following perfusion with high-potassium saline ($[K^+]_{out} = 95$ mM; orange), the resting membrane potential (V_m) increases and the AHP is abolished.

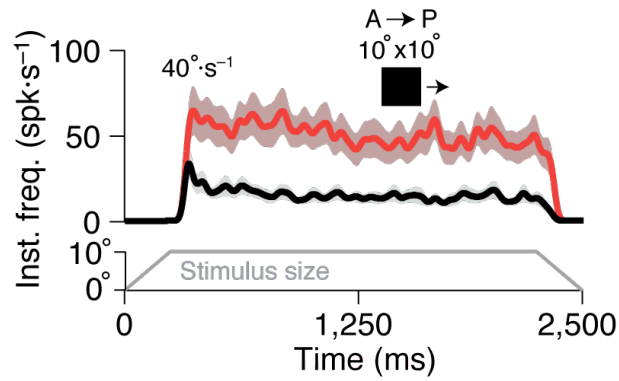


Supplementary Figure 4. The pharmacology of the SK-like K_{Ca} conductance in the LGMD differs from that of vertebrate SK conductances. **(a)** Neither scyllatoxin (STX), UCL-1684, nor NS309 yielded significant changes in f_0 ($p = 0.250$, $p = 0.143$ and $p = 0.393$, respectively; $N=3$ animals each). **(b)** STX, UCL-1684, and NS309 did not produce a significant effect on f_{ss} either ($p = 0.393$, $p = 1$, $p = 0.393$, respectively). **(c)** Similarly, STX, UCL-1684, and NS309 did not yield significant changes in AHP magnitude ($p = 0.143$, $p = 1$, and $p = 0.393$, respectively). Same data analysis and presentation as in **Supp. Fig. 1**. See **Supplementary Pharmacology** for details.

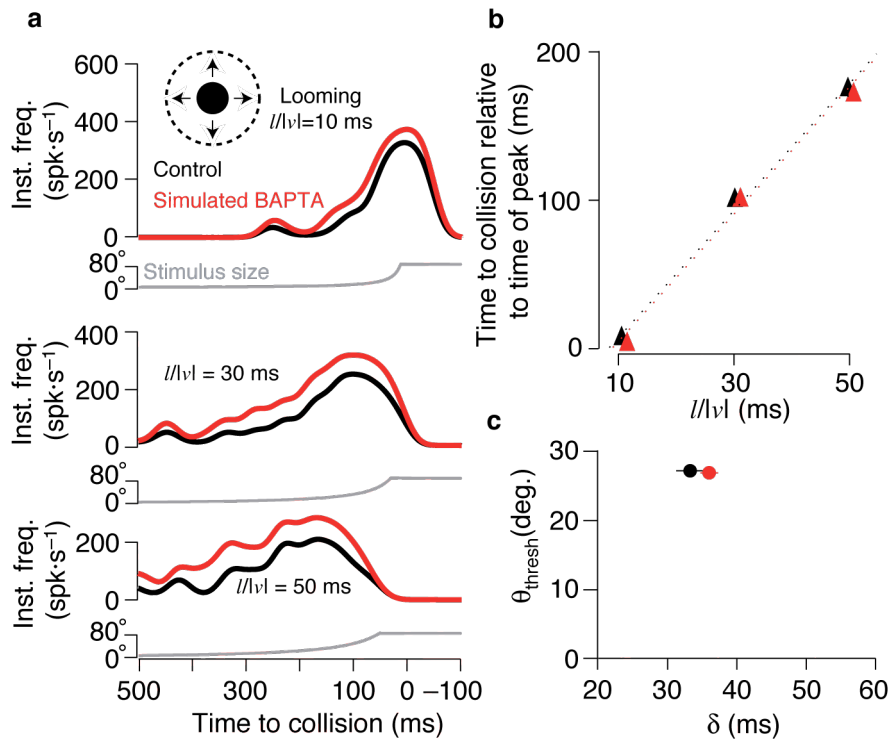
Supplementary Figure 5



Supplementary Figure 5. Blocking spike frequency adaptation in the LGMD by intracellular BAPTA iontophoresis enhances the responses to translating stimuli across all directions, velocities, and stimulus sizes tested. **(a-c)** Instantaneous firing rates averaged across five animals (five trials per condition per animal; N=25 trials total) showing responses to translating squares and rectangles before (black) and after (red) BAPTA iontophoresis. Response s.e.m. is indicated with an envelope of lighter shade. The region of steady-state response (shaded) was used to compute the summary data in **Table 1**. For each stimulus, 3 velocities were tested: 40°, 80°, and 160° s⁻¹. Three stimuli are shown: 10° × 10° squares moving in an AP **(a)** and PA **(b)** direction, and 10° × 80° rectangles moving in an AP direction **(c)**. Each stimulus crossed 80° of visual space from azimuth of 50° to 130°, centered at an elevation of 0° (i.e., equatorial). The size of the stimulus in the azimuth direction as a function of time is indicated at the bottom of each panel.



Supplementary Figure 6. LGMD compartmental model without feed-forward inhibition yields stronger response following simulated BAPTA iontophoresis. Gaussian-convolved ($\sigma = 20$ ms) average response of the model to simulated translation of a $10^\circ \times 10^\circ$ square in the anterior-posterior (AP) direction at 40° s^{-1} before (black) and after (red) simulated BAPTA iontophoresis. Grey outlines show s.e.m. envelopes (N=25 trials). Variability stemmed from simulated synaptic noise and timing jitter; see Methods).



Supplementary Figure 7. Simulated BAPTA iontophoresis has little effect on responses to looming stimuli in LGMD model. **(a)** Simulated responses to looming with $l/|v|=10, 30$ and 50 ms (from top to bottom). Black and red lines show instantaneous firing rate before and after simulated BAPTA iontophoresis, respectively ($N=25$ trials; noise as described in Methods). f_{max} increased from 329 ± 1 to 377 ± 1 , 248 ± 2 to 314 ± 1 , and 208 ± 3 to 284 ± 2 spk s^{-1} for $l/|v|=10, 30$ and 50 ms, respectively (changes of 14, 26, and 37%). $\langle f \rangle$ increased from 64 ± 1 to 87 ± 1 , 102 ± 1 to 153 ± 1 , and 95 ± 1 to 155 ± 1 spk s^{-1} for $l/|v|=10, 30$ and 50 ms, respectively (changes of 36, 51, and 62%). **(b)** Firing rate peak relative to collision time versus $l/|v|$, before (black) and after (red) simulated BAPTA iontophoresis. Solid lines indicate s.e.m. Dotted lines represent linear fits. The magnitude of peak time shifts due to simulated BAPTA were comparable to *in vivo* shifts: from 5.6 ± 0.4 ms (mean \pm s.e.m.) to 1.7 ± 0.2 ms, 104.1 ± 2.0 ms to 101.5 ± 2.3 ms, and 182.2 ± 5.9 ms to 169.9 ± 3.1 ms for $l/|v|=10, 30$ and 50 ms, respectively. **(c)** Threshold angle (θ_{thresh}) as a function of delay to firing rate peak (δ). Again, simulated BAPTA iontophoresis had little effect on θ_{thresh} (shift from $35.1 \pm 2.6^\circ$ to $35.1 \pm 1.5^\circ$) or δ (shift from 26.1 ± 0.8 ms to 27.0 ± 0.4 ms). Same conventions as in **b**.

Supplementary Methods: The Three-Compartment Model

The three-compartment model was implemented by modifying a two-compartment pyramidal cell model²³. The reader is referred to this earlier work for a detailed description of the basic model. Data from our previous work was incorporated to estimate the model parameters^{16,17}. The three compartments simulated the dendrites, the region where the K_{Ca} conductance was localized, and the axon. All three compartments had a leak conductance ($g_{leak} = 0.11$ mS/cm², $E_{leak} = -75$ mV). The compartments had areas of $A_{dend} = 5 \times 10^{-4}$ cm², $A_{KCa} = 5 \times 10^{-5}$ cm², and $A_{axon} = 9.5 \times 10^{-4}$ cm² and were connected as illustrated in **Figure 6a** (inset) using the following coupling conductances: $g_{dend, KCa} = 16.12$ mS/cm², $g_{KCa, dend} = 1.62$ mS/cm², $g_{KCa, axon} = 0.66$ mS/cm², and $g_{axon, KCa} = 12.30$ mS/cm², where $g_{a,b}$ is the conductance from a to b ^{S1}.

Voltage-dependent conductances were simulated using the Hodgkin-Huxley formalism, with the change in a given gate's opening probability determined by $dq/dt = \phi_q [q_{ss}(V_m) - q(t)] / \tau_q(V_m)$. In this equation, ϕ_q is a temperature-dependent scaling factor controlling the overall kinetics of the gate; q_{ss} is the steady state open probability of the gate and τ_q its time-constant of relaxation. The dendritic compartment contained an inward rectifying current (I_h ; $g_{max} = 0.4$ mS/cm²; $E_h = -35$ mV), and was the site of simulated current injection and excitatory synaptic input. The inward rectifying conductance was modeled with $I_h(t) = g_{max} \cdot h(t) \cdot (V_m - E_h)$, with $h(t)$ being the gating variable. The gating variable's time constant and steady state opening probability were governed by the equations $\tau_h(V_m) = 1 / \{0.0018 \cdot \exp[(V_m + 86.6) / -47.5] + 0.0097 \cdot \exp[(V_m + 85.2) / 17.7]\}$ and $h_{ss}(V_m) = 1 / \{1 + \exp[(V_m + 92) / 27.4]\}$, respectively, derived by fitting to previously obtained data¹⁶. The K_{Ca} compartment possessed a voltage-gated calcium current (I_{Ca} ; $g_{max} = 1$ mS/cm²; $E_{Ca} = 90$ mV) and a calcium-sensitive potassium current (I_{AHP} ; $g_{max} = 50$ mS/cm²; $E_K = -80$ mV). Decline in free calcium was simulated as a first order process with a time constant $\tau_{Ca} = 132$ ms²³. To simulate intracellular BAPTA iontophoresis τ_{Ca} was reduced to 20 ms. The influx parameter α converting current density to changes in calcium concentration, $[Ca^{2+}]_{in}$, was assigned a value of $0.12 \mu M(\text{ms } \mu A)^{-1} \text{cm}^2$. An effective K_D of 35 μM was employed for

the dependence of I_{AHP} on calcium concentration. I_{Ca} was modeled using $I_{\text{Ca}}(t) = g_{\text{max}} \cdot k(t) \cdot (V_m - E_{\text{Ca}})$, with $k(t)$ being the gating variable. The time constant and steady state opening probability of the gating variable were governed by the equations $\tau_k(V_m) = 2.5 + 7.5 / \{1 + \exp[(V_m + 10) / -5]\}$ and $k_{\text{ss}}(V_m) = 1 / \{1 + \exp[(V_m + 25) / -3]\}$, respectively. This conductance was modified from the original model²³ to reproduce the rate of adaptation observed in the LGMD. The conductances of the axonal compartment consisted of a fast inactivating sodium (I_{Na} ; $g_{\text{max}} = 90 \text{ mS/cm}^2$; $E_{\text{Na}} = 70 \text{ mV}$) and a delayed-rectifier (I_{KDR} ; $g_{\text{max}} = 22 \text{ mS/cm}^2$; $E_{\text{K}} = -80 \text{ mV}$) responsible for action potential generation. The kinetics of these conductances were accelerated relative the original model²³ to reproduce peak firing rates observed in the LGMD by scaling I_{Na} 's activation, I_{Na} 's inactivation, and I_{KDR} 's gating time constants by factors of 0.25, 0.3, and 0.35, respectively.

We simulated visual input to the LGMD based on detailed morphological data about the locust compound eye, synaptic strength estimates from an earlier study using a multi-compartmental LGMD model^{2,17}, and data showing differential timing of excitation and feed-forward inhibition¹⁵. The number of ommatidia activated by a simulated object's leading or trailing edge was obtained by scaling the change in stimulus size for a given time step (matched to the 5 ms time step of the video monitor) with the location-appropriate sampling density of visual axes by the locust eye. An acceptance half-angle of 2.5° per ommatidium was assumed^{S2}. Each ommatidial activation triggered 5 excitatory and 1 inhibitory synapses, having maximal unitary synaptic conductances of 0.47 mS/cm^2 and 6 mS/cm^2 , respectively. To simulate LGMD response latency, two delay functions based on a sigmoid were employed to match the previously observed difference in latencies between feed-forward inhibition and excitation¹⁵. Specifically, the latency was $t_{\text{delay}} = d_{\text{offset}} + d_{\text{max}} / (1 + \exp((n_{\text{syns}} - d_{1/2}) / d_{\text{slope}}))$, where n_{syns} is the number of synapses activated at a given time step and d_{offset} , d_{max} , $d_{1/2}$ and d_{slope} had values of 50 ms, 50 ms, 0 ms and 10 ms/syn for excitatory synapses and 80 ms, 120 ms, 20 ms and 100 ms/syn for inhibitory synapses. Variability was introduced to all synapses by a random temporal jitter in synaptic activation drawn from a normal distribution ($\mu = 0 \text{ ms}$, $\sigma = 5 \text{ ms}$) and by a spatial angular jitter of visual axes also drawn from a normal distribution ($\mu = 0^\circ$, $\sigma = 10^\circ$). Twenty-five runs were averaged for each simulation condition.

Excitatory ($E_{\text{rev}} = 0 \text{ mV}$) and inhibitory ($E_{\text{rev}} = -75 \text{ mV}$) synapses were simulated with an

alpha-function having $\alpha = 0.3$ ms and $\alpha = 2$ ms, respectively. To simulate background synaptic noise in the LGMD, each excitatory and inhibitory synapse fired at a rate of 0.05 and 0.5 Hz, respectively, with a uniform probability. These spontaneous events had a much smaller maximal conductance of 0.05 and 0.047 mS/cm² for inhibition and excitation, respectively, to simulate spontaneous vesicular fusion. They were employed in both visual and current injection simulations. Both visual and spontaneous excitatory synaptic input was delivered to the dendritic compartment, ignoring the electrotonically extensive structure of the neuron¹⁷. Inhibitory synaptic input arrived at the K_{Ca} compartment, to conform with the observed morphology of the neuron (**Figure 5**). Current was also injected in the dendritic compartment, after dividing the current value by dendritic surface area. All simulations were performed using MATLAB's `ode23` ordinary differential equation solver, a 3(2) Runge-Kutta scheme^{S3}, on a PC running Linux. Computer files implementing the model are available from ModelDB (<http://senselab.med.yale.edu/modeldb>).

Supplementary Pharmacology: Additional SK Channel Drugs

Apamin has been shown to be a specific and selective SK channel blocker in several preparations. However, apamin is thought to be ineffective in insects²⁸, in agreement with our own pharmacological experiments (**Fig. 2**). We thus decided to test additional unrelated agonists and antagonists of SK channels. **Supplementary Figure 4** shows the effect of two additional antagonists, scyllatoxin and UCL1684^{S4}, as well as the agonist NS309^{S5}. None of these compounds had a significant effect on the steady state or peak firing rate of the LGMD, as well as on the amplitude of the AHP. In addition, we tested the agonist 1-EBIO that is thought to act similarly to NS309^{S1}, but be less potent (n = 2 animals, 100 mM dissolved in DMSO; final concentration: 5 mM). As could be expected in light of the NS309 results, we found no effect of 1-EBIO on any spike frequency adaptation parameters of the LGMD (not shown). Finally, we tested in one animal the antagonist d-tubocurarine³⁸ (20 mM dissolved in distilled H₂O; final concentration: 1 mM). Because d-tubocurarine also blocks the nicotinic acetylcholine receptors that provide excitatory inputs to dendritic field A of the LGMD, its potential effect on SK channels may be confounded with an increase in membrane resistance caused by the inactivation of a large fraction of the synaptic input received by the LGMD. We thus first applied the nicotinic blocker mecamylamine^{S6} (final concentration: 5mM, dissolved in distilled H₂O), and studied the effect of subsequent application of d-tubocurarine on the firing and membrane potential properties of the LGMD, but found none (not shown).

Although an SK channel gene has been identified in insects^{S7}, to our knowledge no effective agonists or antagonists are known. In addition to confirming the ineffectiveness of apamin, the pharmacological experiments reported here suggest that scyllatoxin, NS309, UCL1684, 1-EBIO and d-tubocurarine may also be ineffective against insect SK channels. Thus, further experiments will be needed to characterize the pharmacology of SK channels in insects. Substantial differences in the pharmacological properties of vertebrate and insect channels have been reported before, for example GABA_A receptors in insects are completely insensitive to bicuculline, in contrast to vertebrate ones^{S8}.

Supplementary References

- S1. Pinsky, P.F. & Rinzel, J. Intrinsic and network rhythmogenesis in a reduced Traub model for CA3 neurons. *J. Comput. Neurosci.* **1**, 39-60 (1994)
- S2. Wilson, M. Angular Sensitivity of Light and Dark Adapted Locust Retinula Cells *J. Comp. Physiol.* **97**, 323-8 (1975)
- S3. Bogacki, P. & Shampine, L.F. A 3(2) Pair of Runge-Kutta Formulas. *Applied Math Letters* **2**, 315-325 (1989)
- S4. Liégeois, J.F. *et al.* Modulation of small conductance calcium-activated potassium (SK) channels: a new challenge in medicinal chemistry. *Curr. Med. Chem.* **10**, 625-47 (2003)
- S5. Strøbaek, D. *et al.* Activation of human IK and SK Ca^{2+} -activated K^{+} channels by NS309 (6,7-dichloro-1H-indole-2,3-dione 3-oxime). *Biochim. Biophys. Acta.* **1665**, 1-5 (2004)
- S6. Trimmer, B. & Weeks, J.C. Effects of nicotinic and muscarinic agents on an identified motoneurone and its direct afferent inputs in larval *Manduca sexta*. *J. Exp. Biol.* **144**, 303-337 (1989)
- S7. Littleton, J.T. & Ganetzky, B. Ion channels and synaptic organization: analysis of the *Drosophila* genome. *Neuron* **26**, 35-43 (2000)
- S8. Rauh J.J., & S.C., Sattelle D.B. Pharmacological and biochemical properties of insect GABA receptors. *Trends Pharmacol. Sci.* **11**, 325-9 (1990)